Geophys. J. Int. (2008) **175,** 1141–1153 doi: 10.1111/j.1365-246X.2008.03952.x

A possible mechanism for the spatial distribution of seismicity in northern Gulf of Mexico

Abhijit Gangopadhyay[1] and Mrinal K. Sen[2]

[1]*BP America,* 501 *Westlake Park Boulevard, Houston,* TX 77079, *USA. E-mail: Abhijit.Gangopadhyay@bp.com*
[2]*Institute for Geophysics, John A. and Katherine G. Jackson School of Geosciences, University of Texas at Austin, J. J. Pickle Research Campus, Bldg.* 196 *(ROC),* 10100 *Burnet Road, Austin,* TX 78758*, USA*

Accepted 2008 August 26. Received 2008 August 15; in original form 2008 January 2

SUMMARY

In an aseismic part of northern Gulf of Mexico (GOM), three earthquakes of M_s 5.2, M_w 4.6 and M_w 5.8 occurred between 2006 February and September. These earthquakes raised concerns because of their proximity to locations of active hydrocarbon production, and potential for tsunami generation, prompting investigations about their causes. Herein, we test a hypothesis using 2-D and 3-D models, where stress concentration due to contrast in mechanical properties between the salt deposits and surrounding sediments in the northern GOM, driven by background tectonic loading, may have triggered these earthquakes in particular, and cause earthquakes in the northern GOM in general. We perform the mechanical modelling by a 'distinct element method' implemented through commercially available computer programmes called 'Universal Distinct Element Code (UDEC)' and 'Three-Dimensional Distinct Element Code (3DEC)'. Our models consist of a simplified regional outline of the salt bodies surrounded by sediments. We assign mechanical properties to the salt and sediments based on known geology and seismic velocities. We load the models tectonically for a year, and observe the patterns of resulting shear stresses. The results of modelling suggest that some locations of relatively high shear stress correlate well with the spatial distribution of seismicity in the northern GOM, thereby suggesting a possible causal association.

Key words: Numerical approximations and analysis; Spatial analysis; Seismicity and tectonics; Dynamics: seismotectonics; Mechanics, theory, and modelling; North America.

INTRODUCTION

Geologically, the Gulf of Mexico (GOM) is an extensively studied region due to its immense hydrocarbon productivity and potential (e.g. Pan *et al.* 2006). It continues to remain an excellent natural laboratory to study fundamental sedimentation processes, petroleum systems and related tectonics (e.g. Dokka *et al.* 2006; Matava 2006). Although, evolution of the GOM through geological time is well established (e.g. White 1980; Pindell 1985; Winker & Buffler 1988; Salvador 1991; Hall & Najmuddin 1994; Marton & Buffler 1994; Bird *et al.* 2005), there is debate over whether it is tectonically active or passive in the present day (e.g. Reed 1994, 1995; Sarwar 2002). The latter opinion is particularly due to the general paucity of seismicity in the central and northern GOM (e.g. Frohlich 1982; Nunn 1985; Dokka *et al.* 2006). However, between 2006 February and September, three earthquakes of M_s 5.2, M_w 4.6 and M_w 5.8 occurred in the northern GOM within ∼100–530 km offshore Louisiana (e.g. Nettles 2006; United States Geological Survey—National Earthquake Information Center 2006), indicating that the region may instead be tectonically active. In addition, analyses of recent geodetic data (e.g. Dokka 2006; Dokka *et al.* 2006) suggest ongoing tectonic activity at the northern edge of GOM in offshore Louisiana.

The earthquakes in northern GOM during 2006 occurred in a seismically quiet area. Their proximity to locations of active oil and gas production, and speculations about their potential for tsunami generation, caused widespread interest in additional investigations about their possible causes. In this study, we test a hypothesis wherein stress concentration due to contrast in mechanical properties between the salt deposits and surrounding sediments in the northern GOM, driven by background tectonic loading, may have triggered these earthquakes in particular, and cause occasional earthquakes in the northern GOM in general. The hypothesis is based on earlier independently published analytical, modelling and case studies that discussed mechanisms of stress concentration involving bimaterials with different mechanical properties and associated rupture along their interface (e.g. Donnell 1941; Campbell 1978; Ben-Zion 2001; Ben-Zion & Huang 2002; Gangopadhyay 2005; Brietzke & Ben-Zion 2006; Stevenson *et al.* 2006; Ampuero & Ben-Zion 2008). For the purpose, we use a numerical modelling technique called the 'distinct element method' (Cundall 1971). We implement the method using commercially available computer programmes called 'Universal Distinct Element Code (UDEC)' in two dimensions, and 'three-dimensional Distinct Element Code (3DEC)' in three dimensions (UDEC 1999; 3DEC 2003). In this paper, we present our study using a multifold approach as follows: first, we

review the existing causal mechanisms of GOM earthquakes, second, we discuss the numerical modelling methodology in general as applicable to understanding geological and tectonic situations, third, we demonstrate by simple examples that using our numerical modelling technique we can duplicate the results of earlier analytical studies which led to the hypothesis that we test herein, and finally, we apply our technique in two and three dimensions to test the hypothesis in the case of northern GOM. We provide details of important computational steps involved in the modelling in Appendix.

A note on the scope of this study

Given the existence of extensive studies and detailed mapping of salt bodies in the GOM, both in two and three dimensions, it is important to mention at the outset that in this study we use very simplified 2-D and 3-D outlines of the salt bodies for our models. A reason for this simplification is the limitation imposed by the educational version of the programmes that we use. We emphasize that the focus of this study is to demonstrate and bring to the attention of the hydrocarbon exploration and production community, application to the northern GOM of a phenomenon that is extensively studied in the earthquake community, and which appears to be a promising candidate to explain the seismicity of the northern GOM. We do not intend to imply that the hypothesis tested in this study is the only cause of earthquakes in northern GOM.

REVIEW OF PROPOSED CAUSAL MECHANISMS OF GOM EARTHQUAKES

Although small earthquakes ($M < 5.0$) in the northern GOM occur sporadically over time, the occurrence of a M 5.0 earthquake on 1978 July 24, which was also the best recorded earthquake at that time, spawned studies of the causes of seismicity in this relatively aseismic part of the GOM. Frohlich (1982) obtained a reliable location for this earthquake and studied its focal mechanism thereby suggesting that it may be related to stresses associated with the down-warping of the lithosphere caused by accumulation of sediments from the Mississippi river. He also suggested that other earthquakes in the region occurred near boundaries of distinct geological regions and hence could be associated with areas of pre-existing weakness in the crust. To analyse the state of stress in the northern Gulf coast, Nunn (1985) performed simple flexural calculations. His results supported the conclusion of Frohlich (1982) that bending stresses caused by rapid sediment loading may be a potential cause of infrequent earthquakes in the northern GOM. Using an illustration of Mohr circles, Talwani & Rajendran (1991) concluded that additional horizontal stresses offshore overcame the vertical stress thereby resulting in a thrust mechanism for the 1978 July 24 earthquake.

Owing to infrequency of earthquakes in the northern GOM, there was a hiatus in studies investigating their causes during the last decade, until the occurrence of the earthquakes in 2006. Concerns about their tsunami generation potential and impact on existing and future hydrocarbon exploration installations caused geoscientists from both academia and industry to investigate their causes. At a workshop organized for the purpose in the last quarter of 2006 by the Society of Exploration Geophysicists (SEG), and the Offshore Technology Conference (OTC) in Spring 2007, several potential causes of these earthquakes were proposed by various researchers. However, active plate tectonics was ruled out as a cause. The 2006 September 10 event was almost unanimously considered a tectonic earthquake because of its typical 'earthquake-like' signatures, however, two potential causes were most favoured for the anomalous 2006 February 10 event. These were possible sliding on Sigsbee salt and occurrence of a landslide (Nettles 2007). The latter cause was supported by the fact that modellings of waveforms of the 2006 February 10 event (which were depleted in high frequency) recorded at different seismic stations were best achieved using a landslide source rather than a typical double-couple earthquake source (Nettles 2007). Comparison of this event's characteristics was also made with those of landslide events in the Norwegian fjords to investigate any commonality. A fracture mechanics approach to modelling a landslide was also proposed. The possible causal mechanism we present herein was also discussed at the SEG workshop in 2006.

Next, we describe the modelling technique used in this study as applicable to understanding geological and tectonic problems in general.

DISTINCT ELEMENT METHOD

The distinct element method is a numerical modelling technique for analysis of discontinuous media. The geological framework of the region under investigation is included in a model built using a set of rock blocks that contain the faults within them. The faults are treated as discontinuities in the programme. The method addresses the mechanical behaviour of both the rock blocks and faults. The computations are based on a finite-difference formulation of Newton's law of motion. The rock blocks can either be rigid or deformable. The deformable blocks are divided into a mesh of triangular (2-D) and tetrahedral (3-D) finite-difference zones using an automatic built-in mesh generator. Each of these zones behaves according to a prescribed constitutive relation. The faults can move in both the normal and shear directions, and their relative motion is governed by force–displacement relations. Appropriate elastic moduli and density values are assigned to the blocks, whereas the faults are assigned normal and shear stiffnesses, friction angles and cohesion. The programmes consist of a suite of constitutive relations for the blocks and faults to allow simulation of the response of various geological media. To drive the model, an external displacement, velocity or stress field can be used. The equations of motion involved in the model computations are solved progressively in time using discrete time steps. For a model comprising of deformable blocks, the time step is determined by the zone size, fault stiffnesses and elastic moduli of the blocks. The positions, velocities (translational and rotational), displacements, stresses and strains at each node (vertices of the zones) are computed at every time step. The computations continue repetitively until the end of the prescribed tectonic loading period. The resulting final values of stresses, and displacements within the rock blocks and along the faults, are then used for tectonic interpretations. The computational scheme is identical to the finite-difference method for continuum analysis (UDEC 1999; 3DEC 2003; see Appendix for details).

Next, we present test applications of the modelling method and compare the results with those obtained from an earlier analytical study which led to the hypothesis that we test in this paper.

APPLICATION OF THE MODELLING METHOD—CONSISTENCY TESTS

Using the distinct element method implemented in 'UDEC', we construct simple 2-D models of circular and elliptical intrusions

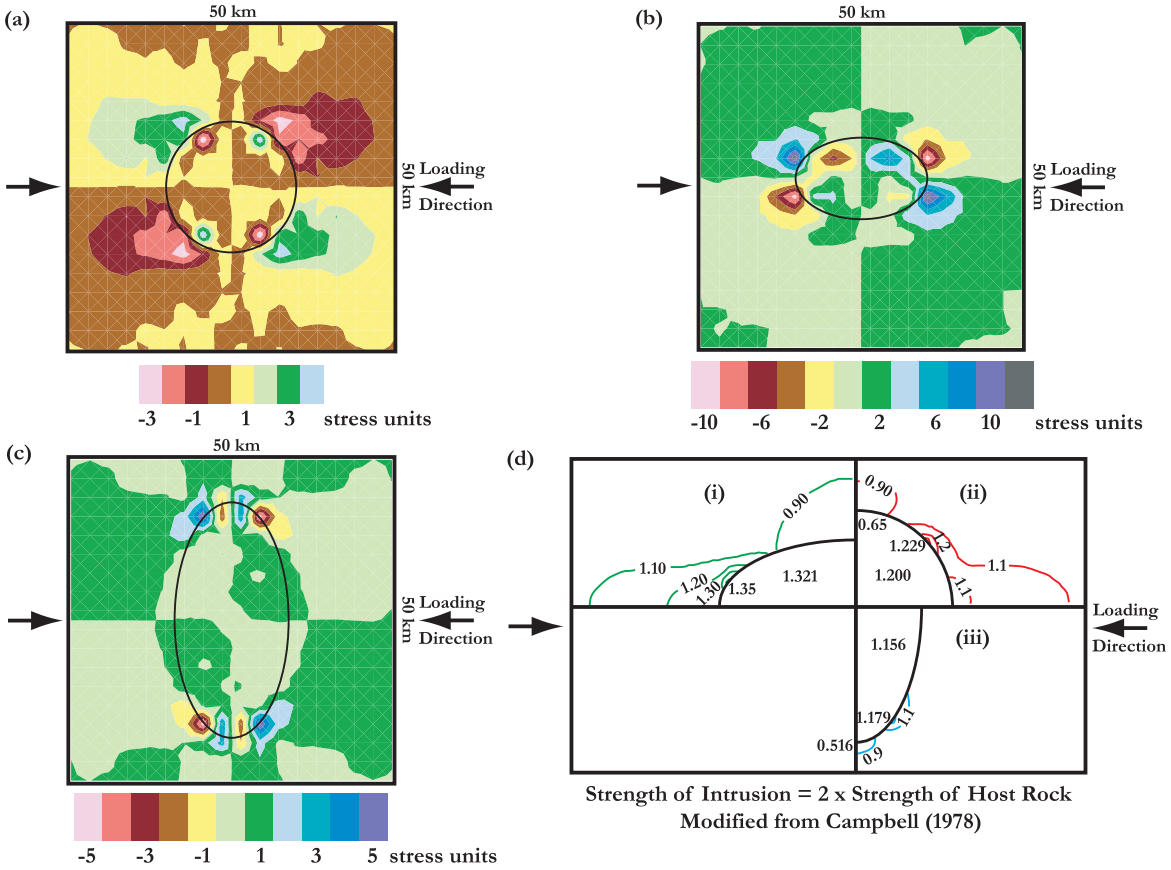

Figure 1. Simple 2-D models constructed using UDEC of (a) circular intrusion, (b) elliptical intrusion with major axis parallel to loading direction and (c) elliptical intrusion with major axis perpendicular to loading direction, surrounded by host rocks. The intrusions are twice as strong as host rocks. Solid arrows represent the direction of loading in each case. Superimposed on the model geometries are shear stress (τ_{xy}) contours obtained after 100 000 cycles of tectonic loading. The numbers alongside the colour scales indicate magnitudes of shear stresses obtained and are only for reference. (d) Plot of shear stress contours obtained analytically by Campbell (1978) following loading of similar shapes of intrusions twice as strong as the host rocks. (i) Represents a quadrant of an elliptical intrusion with major axis parallel to the loading direction, (ii) represents a quadrant of a circular intrusion and (iii) represents a quadrant of an elliptical intrusion with major axis perpendicular to the loading direction. The numbers on the contour lines indicate the magnitudes of stresses. The locations of relatively high shear stresses in (a)–(c) are of importance and are compared with those in (d) for each type of intrusion. Details of comparison are mentioned in the text.

surrounded by host rocks. These are shown in Figs 1(a)–(c). To compare the results of our modelling with those obtained analytically by Campbell (1978), in our models we follow his choice of shape of intrusions, and direction of loading (∼E–W). In Figs 1(a)–(c), we show our models for circular and elliptical intrusions with major axis parallel, and perpendicular to the direction of loading respectively. We choose the dimensions of our models in these examples arbitrarily (50 × 50 units of length), however, these are such that boundary effects do not influence the results of our modelling. Also, following one set of examples discussed by Campbell (1978), in all our models, we consider the intrusions to be twice as strong as the host rocks, and assign their material properties (bulk and shear moduli, and density) based on generic values obtained from previously studied case histories in South Carolina (Stevenson *et al.* 2006). We consider our models to be linear–elastic and isotropic. We load our models tectonically along the horizontal direction for ∼100 000 cycles which is the time taken in these cases for the results to be numerically stable. At the end of the tectonic loading period, we analyse the distribution of shear stresses (τ_{xy}) in our models, and their contours (colour-coded by magnitude) are superimposed on the model geometries as shown in Figs 1(a)–(c). The absolute values of shear stresses in these results are insignificant. However, their relative values at different locations within the models are important for qualitative comparison with the results of the analytical study of Campbell (1978) which are shown in Fig. 1(d).

Comparing Figs 1(a)–(c) with Fig. 1(d), we note that the locations of relatively high shear stresses (positive or negative) are similar. In the case of a circular intrusion, Campbell (1978) obtained highest stresses (∼1.2–1.23 units of stress) at and near the periphery of the intrusion (mostly outside but also inside it) in a ∼NE–SW orientation [Fig. 1d; quadrant (ii)], similar to our results (∼±3 units of stress; Fig. 1a). Using elliptical intrusions, the highest stresses obtained by Campbell (1978) are also at and near the periphery of the intrusions (both outside and immediately inside them), but oriented ∼E–W and ∼WNW–ESE (∼1.32–1.35 units of stress) when the major axis of the intrusion is parallel to the loading direction [Fig. 1d; quadrant (i)], and ∼N–S, and ∼NNE–SSW (∼1.18 units of stress) when the major axis is perpendicular to the loading direction [Fig. 1d; quadrant (iii)]. The locations of relatively high stresses from our modelling results for these shapes of intrusions under identical loading conditions are also similar (∼±10 and ±5 units of stress respectively; Figs 1b and c). Although Campbell (1978) showed contours of stress in one quadrant for each geometrical

shape of intrusion, he obtained similar high stresses in other quadrants for the same type of intrusion, by symmetry. The results of our modelling also show the effects of symmetry (lobes of high stress in every quadrant), oriented ∼NE–SW, and ∼NW–SE for circular, ∼E–W, ∼WNW–ESE and ∼WSW–ENE for elliptical (with major axis parallel to loading direction), and ∼N–S, ∼NNE–SSW and ∼NNW–SSE for elliptical (with major axis perpendicular to loading direction) intrusions (Figs 1a–c). In his analytical study, Campbell (1978) also described cases where the same intrusions were weaker than the host rocks. He again obtained relatively high stresses at and near the periphery of the intrusions, except that they were at different locations around the periphery compared to the cases where the intrusions are stronger than the host rocks. The magnitudes of stress also differed in either set of cases. By his results, Campbell (1978) demonstrated the phenomenon of stress concentration in geological situations, that due to contrast in mechanical properties between intrusions and host rocks, upon background tectonic loading, higher stresses can concentrate preferentially at and near the periphery of the intrusions. He also concluded that this mechanism could generate stresses high enough to cause brittle failure such as in earthquakes, in and around the intrusions. The locations and magnitudes of these high stresses depend on the shape and size of the intrusions, orientation of loading direction and strength of intrusions compared to host rocks (Campbell 1978; Gangopadhyay 2005). Apart from Campbell (1978), similar conclusions are also drawn in more recent analytical and case studies by Ben-Zion (2001), Ben-Zion & Huang (2002), Brietzke & Ben-Zion (2006) and Ampuero & Ben-Zion (2008). In a review of several problems of dynamic rupture relevant to earthquake fault mechanics, Ben-Zion (2001) highlights the importance of a better understanding of such phenomenon along an interface separating different elastic solids. Ben-Zion & Huang (2002) use a 2-D plane strain finite-difference approach to study dynamic rupture on a material discontinuity interface between a compliant elastic layer and a stiffer elastic medium. In a parametric study of 2-D in-plane ruptures, Brietzke & Ben-Zion (2006) document spontaneous migration of dynamic ruptures to the material interface. Ampuero & Ben-Zion (2008) systematically conduct several numerical simulations of in-plane ruptures on a bi-material interface and demonstrate high seismic potency. In summary, all these recent studies show that bi-material interfaces are dynamically considerably weaker than the surrounding solids, since the difference of elastic properties produces dynamic reduction of normal stress, that is, limited to the bi-material interfaces. Due to this additional dynamic weakening, seismicity tends to localize along bi-material interfaces.

The results of modelling these simple cases using our technique (Figs 1a–c) duplicate successfully those of Campbell (1978) (Fig. 1d), and support the conclusions of more recent mathematical simulations (e.g. Ampuero & Ben-Zion 2008). They, therefore motivate the demonstration of the hypothesis by application of the distinct element method technique to model northern GOM. We describe our models specific to northern GOM, next.

DISTINCT ELEMENT MODELS OF THE NORTHERN GULF OF MEXICO

Two-dimensional models

To construct 2-D models of the salt bodies in northern GOM, we use a generalized map of northern GOM as shown in Fig. 2(a) [Gulf Basin Depositional Synthesis (GBDS) Project 2006]. It comprises of the tabular salt canopy bounded to the south by the Sigsbee escarpment. In Fig. 2(b), on a regional scale, we show the geographic area encompassing northern GOM, including the sparse instrumental and historical seismicity (United States Geological Survey—National Earthquake Information Center), and locations of oil and gas platforms for reference. We superimpose the approximate outline of the tabular salt canopy (Fig. 2a) on this regional map as shown in Fig. 2(b). On the same scale, we also show the approximate outline of the entire extent of the salt bodies in northern GOM following Reed (1994), and location of the West Florida escarpment, the latter being host to a majority of earthquakes in the area (Fig. 2b). To provide a reference to the orientation of the stress field in the area, we also show obtained focal mechanisms of the major earthquakes (Frohlich 1982; Pulliam 2006, personal communication; Global Centroid Moment Tensor Catalog 2006).

Based on the outlines of the salt bodies represented in Fig. 2(b), we construct simple 2-D models using the distinct element method implemented in 'UDEC' (Figs 3a–d). The block geometries used in the models include the tabular salt canopy (Galloway 2006; Figs 3a and b), and the entire extent of the salt bodies (Reed 1994; Figs 3c and d), surrounded by sediments. Due to a limitation in 'UDEC' we are unable to have the salt bodies stand-alone within the models. Therefore, as anchors we include major geological structures such as 'Port Isabel fold belt' (Fig. 2) in our models with the tabular salt canopy (Figs 3a and b), and 'West Florida escarpment' in our models with the entire extent of the salt bodies (Figs 3c and d). To minimize boundary effects on the regions of interest, we extend the block boundaries substantially away from them resulting in total model areas of ∼1255 km × 1238 km (Fig. 3a), ∼1255 km × 788 km (Fig. 3b) and ∼2193 km × 1827 km (Figs 3c and d), respectively. These areas well encompass the region between ∼25–31°N latitudes and ∼84–97°W longitudes. The choice of areal extent of the models does not in any way change the conclusions of this study. Gangopadhyay (2006) described observations of shear stress distribution patterns in the blocks obtained from experimental runs of various models wherein their areas were varied. He concluded that the spatial patterns of shear stress distribution in the blocks obtained at the end of the tectonic loading period are not altered by change in the areal extent of the models. To avoid singularities at block corners, we round them with a circle that is tangential to the two corresponding edges at a specified rounding distance from the corner. In practice, the rounding distance is about 1 per cent of the typical block edge length (UDEC 1999). We use the same convention in models in this study. In our 2-D models, we also impose the commonly used plane stress condition. All the blocks in our models are deformable and movable with respect to each other. We divide the blocks into triangular finite-difference zones using a built-in automatic mesh generator that decides the size of the elements based on the block lengths, specified rounding length and the memory availability to perform the computations.

To drive our models, we load them tectonically along the inferred direction of maximum horizontal compression (S_{Hmax}; Fig. 3a–d). Despite almost 20 yr of data collection and widespread application of stress data for issues affecting petroleum exploration and production, little is known about the state of stress in the GOM (Tingay *et al.* 2005). The 'World Stress Map' (Reinecker *et al.* 2005) which is a compilation of up-to-date stress data available globally, shows that in the northern GOM, a uniform stress field is absent. There are several orientations of the maximum horizontal compressive stress (S_{Hmax}) at different locations in the northern GOM (Reinecker *et al.* 2005), and these are believed to result from complex far-field forces, geological structures and mechanical

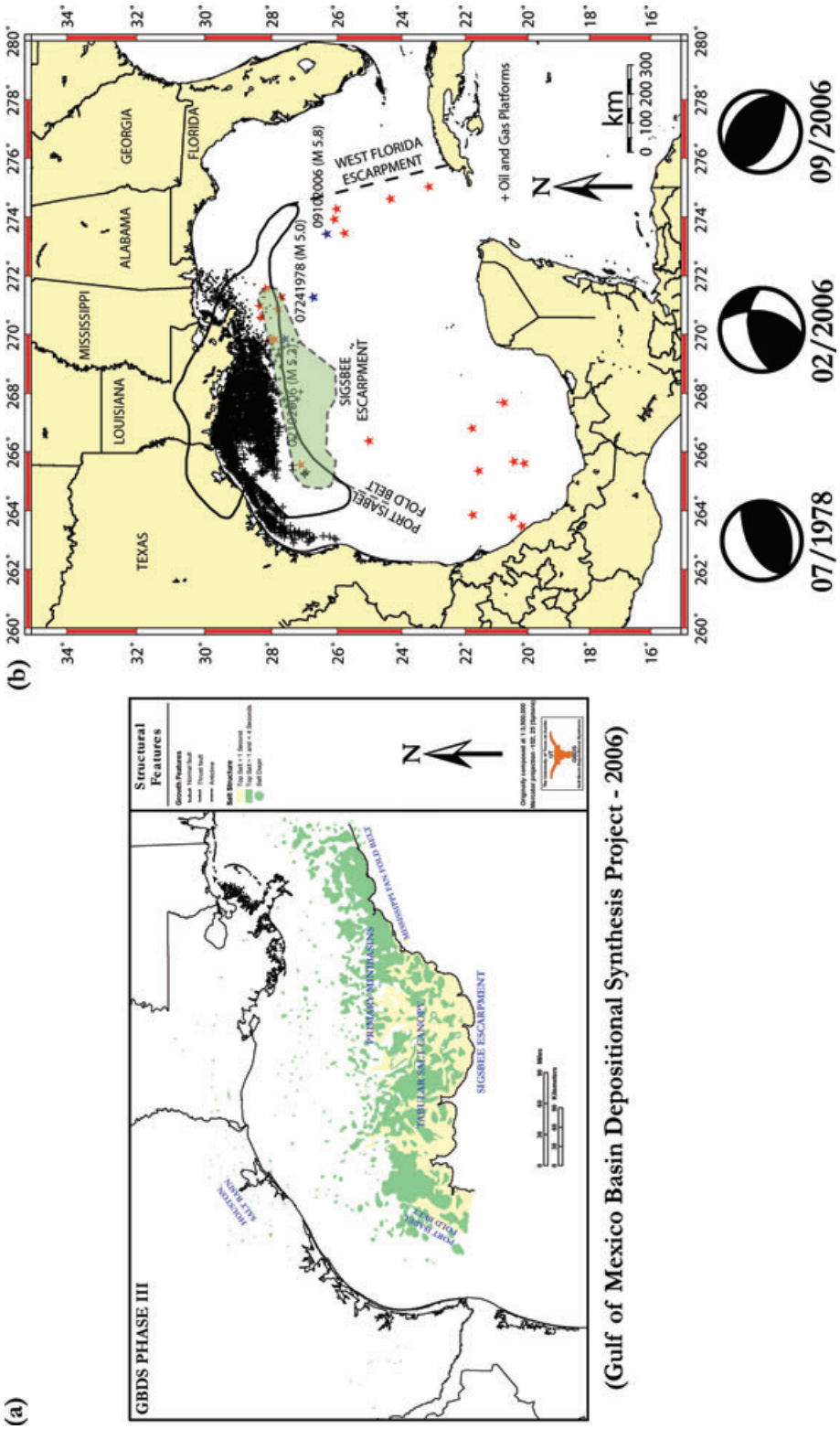

Figure 2. (a) Map of northern Gulf of Mexico showing the location of tabular salt canopy and few major geological structures (modified from 'Gulf of Mexico Basin Depositional Synthesis Project (GBDS)' Galloway 2006). (b) Map of Gulf of Mexico showing generalized extent of salt deposits in its northern part, used in our models. The black outline represents the extent of the exterior salt basin from Reed (1994), and the light-green shaded dashed area represents the tabular salt canopy adapted from (a) (light-green and yellow area). Approximate locations of some important geological structures are indicated on the map. The offshore earthquakes (red stars) from the Advanced National Seismic System (ANSS) and National Earthquake Information Center (NEIC) catalogues are also superimposed on it. The blue stars indicate the locations of the three earthquakes during 2006. The focal mechanisms of the 1978 July 24 (Frohlich 1982), 2006 February 10 (Pulliam 2006, personal communication) and 2006 September 10 (Global CMT catalogue) earthquakes are shown as beach balls.

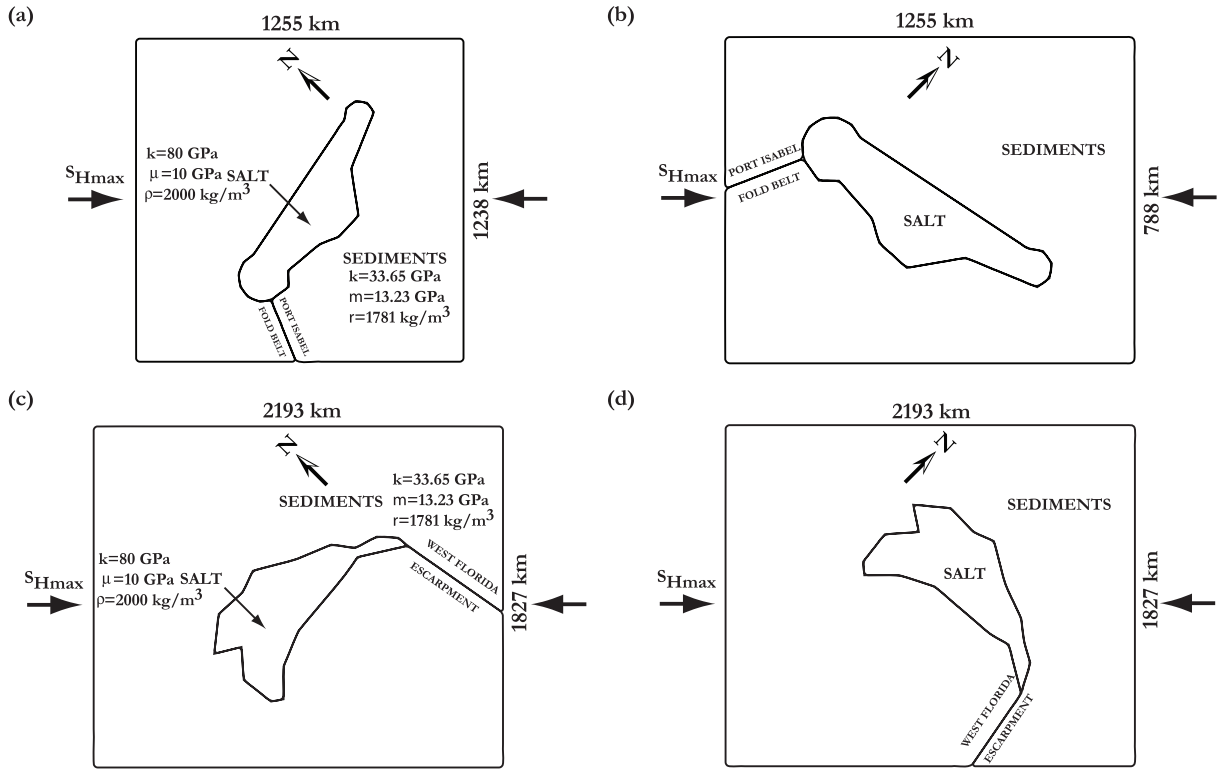

Figure 3. 2-D model geometries used in this study of the salt bodies and sediments surrounding them. The models are constructed using UDEC following outline of tabular salt canopy from 'Gulf of Mexico Basin Depositional Synthesis Project (GBDS)'— Galloway 2006 (a) and (b), and entire extent of salt bodies from Reed (1994) (c) and (d). The solid arrows indicate the direction of tectonic loading which is ∼NW–SE in (a) and (c), and ∼NE–SW in (b) and (d). The representative mechanical properties (bulk and shear moduli, k and μ, and density, ρ) used in modelling for the salt bodies and sediments are also indicated in (a) and (c).

contrasts (Tingay *et al.* 2005). Predominant orientations of S_{Hmax} are ∼NW–SE, N–S and NE–SW. Focal mechanisms of earthquakes also provide additional constraints on the prevailing stress field in a region. The focal mechanisms of the 1978 July 24, and 2006 February 10 , earthquakes in the northern GOM (Frohlich 1982; Pulliam 2006, personal communication) indicate that S_{Hmax} (coincident with the direction of the *P*-axis) is oriented ∼NW–SE. On the other hand, the focal mechanism of the 2006 September 10 earthquake further southeast, indicate that S_{Hmax} is oriented ∼NE–SW. Therefore, in either of our set of models we use both orientations of S_{Hmax}, individually, as the tectonic loading direction. However, our 2-D computer programme allows us to apply external stresses in either the horizontal (E–W) or N–S orientations. Therefore, in each case we rotate our model including the salt body appropriately so as to apply the S_{Hmax} in the E–W direction. Figs 3a and b show the models with tabular salt canopy and effectively NW–SE and NE–SW tectonic loading, whereas Figs 3(c) and (d) show the models with the entire extent of salt bodies and effectively NW–SE and NE–SW tectonic loading. We apply the tectonic loading as a boundary condition and use ∼40 MPa as its magnitude. We obtain this value from the range of S_{Hmax} (∼39.6–43 MPa) obtained at a depth of ∼2 km by Peška & Zoback (1995), where they illustrate by a case study from the Eugene Island Block 330, offshore Louisiana, in GOM, that it is possible to utilize observations of borehole failures to determine the magnitude and orientation of the stress tensor in areas such as offshore sedimentary basins where drilling inclined well bores is quite common. We assume that ∼40 MPa is a representative value of S_{Hmax} in the region of interest in this study. The behaviour of the blocks is dependent on the value of this applied background loading stress. However, the calculated stresses scale linearly if a different value of the loading stress is used. Moreover, the absolute values of the calculated stresses are insignificant for the purpose of this study, instead their relative values at different locations in the models are relevant. Also, in these 2-D models, due to the absence of the third dimension, we assume that the magnitude of S_{Hmax} is unchanged with depth, and do not take into account the vertical stress.

Input parameters for the model calculations include bulk and shear moduli, and density of the blocks, and friction angle, normal and shear stiffnesses, and cohesion of the faults. In a study of salt tectonics using finite-element simulations of a reaction, transport and mechanics model, Tuncay & Ortoleva (2001) used salt bodies with a halite composition having bulk and shear moduli of 80 and 10 GPa, respectively, and density of 2000 kg m^{-3}. In our models, we follow Tuncay & Ortoleva (2001) and use these representative values for the salt bodies. For the sediments surrounding the salt bodies, we compute the bulk modulus using generic formulae described in detail in Gangopadhyay *et al.* (2004), wherein we incorporate the density, and Poisson's ratio. In an *in situ* evaluation of the response of seafloor sediments to passive dynamic loads at a site in the GOM (∼27.3°N, 94.3°W) near the epicentral region of the 1978 July 24 earthquake, Huerta-Lopez *et al.* (2003) obtained an average shear modulus of 13.23 GPa, density of 1781 kg m^{-3}, and Poisson's ratio of 0.32 for the sediments. Using generic formulae described in Gangopadhyay *et al.* (2004), we obtain the bulk modulus for the sediments as 33.65 GPa. We use these values of bulk and shear moduli and density for the surrounding sediments in our models. In the 2-D models shown in Fig. 3, we consider the 'Port Isabel fold belt' and 'West Florida escarpment' as discontinuities (faults). To

our knowledge site-specific mechanical properties for these structures are unavailable. Therefore, for these we use normal and shear stiffnesses (101 and 76 GPa m^{-1}, respectively) based on laboratory studies of typical rock samples following Rosso (1976), as detailed in Gangopadhyay *et al.* (2004). We also assign a friction value of 0.5 to these structures, adapted from experimental results on typical rock types reported by Barton (1976), and consider them to be cohesionless. We emphasize that calculations with different values of these mechanical properties scale our results linearly, and do not change the general conclusions of this study. In our models we use the simplest constitutive relations for the blocks (linear, elastic and isotropic), and discontinuities (Coulomb Slip Failure model). Finally, we run our models for a tectonic loading time of 1 yr. We are unable to run our models for a more geologically realistic tectonic loading time because we use an educational version of the code that has memory restrictions for running such models. Since we use a linear, elastic and isotropic constitutive relation, the absolute values of calculated stresses scale linearly if we use a greater tectonic loading time. However, as we note earlier, the absolute values of the calculated stresses are insignificant for the purpose of this study, instead their relative values at different locations in the models are relevant. Results using a greater loading time therefore do not in any way alter the conclusions of this study. We analyse the resulting shear stresses, which we describe next.

Results of two-dimensional modelling

We analyse outputs from the modelling in terms of the resulting shear stresses (τ_{xy}) in the modelled blocks in response to the externally applied load. To compare these stresses with the locations of seismicity, we assume their temporal stationarity. In each case, shear stress values obtained from the modelling results at each node of the model mesh are contoured, and superimposed on the block geometry as shown in Figs 4(a)–(d). Positive and negative values are associated with counter-clockwise and clockwise rotation of the blocks, respectively. We emphasize that the absolute values of shear stress obtained in this study are insignificant but their relative values at different locations within the models are instructive. First, we present the results of our modelling and discuss their tectonic implications later.

Fig. 4(a) shows the contours of shear stress obtained after an ∼NW–SE tectonic loading of 1 yr, of the model containing the tabular salt canopy. We contour the shear stress values at the nodes with an interval of 20 stress units, and these range between −60 and 100 units of stress (Fig. 4a). The shear stresses in most of the areas within the model vary within ∼0 and 20 units of stress, except at and around the eastern and western edges of the tabular salt canopy, both inside and immediately outside it (Fig. 4a). In these areas, the shear stresses are higher (−40–60 and 40–100 units of stress;

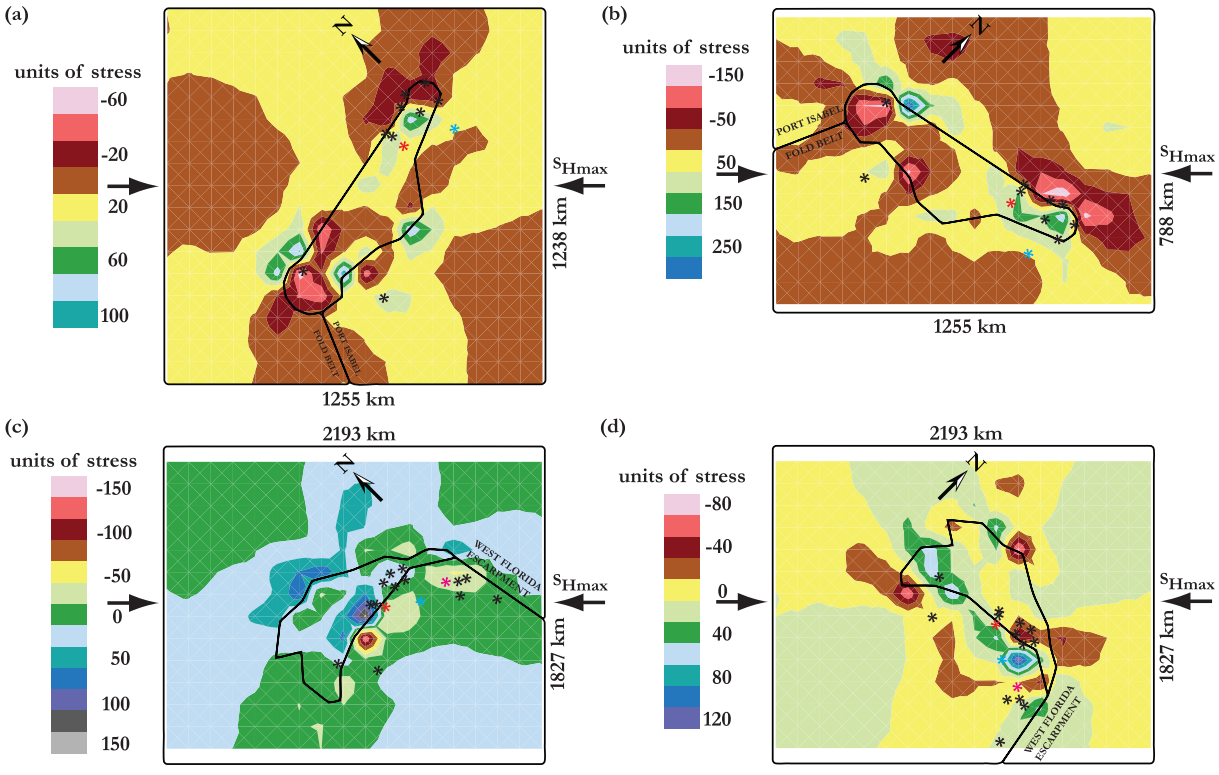

Figure 4. Contours of shear stress (τ_{xy}) obtained from our 2-D modelling results using UDEC after a tectonic loading time of 1 yr for geometries of the salt bodies and sediments surrounding them, constructed following outline of (a) tabular salt canopy from 'Gulf of Mexico Basin Depositional Synthesis Project (GBDS)' Galloway 2006, and ∼NW–SE tectonic loading, (b) tabular salt canopy from 'Gulf of Mexico Basin Depositional Synthesis Project (GBDS)' Galloway 2006, and ∼NE–SW tectonic loading, (c) entire extent of salt bodies from Reed (1994), and ∼NW–SE tectonic loading, (d) entire extent of salt bodies from Reed (1994), and ∼NE–SW tectonic loading. The solid arrows indicate the direction of tectonic loading in each case. The seismicity (stars) is superimposed on the model geometries. Particular earthquakes are shown as coloured stars: 1978 July 24 (blue), 2006 February 18 (red) and 2006 September 10 (magenta).

Fig. 4a). Also, near the southern edge of the tabular salt canopy there are pockets of relatively high shear stresses, east of Port Isabel fold belt (−40 and 40–80 units of stress; Fig. 4a). These areas within the model where stresses are relatively elevated are potential locations of seismicity.

In Fig. 4(b), we show the shear stress contours obtained after tectonic loading of the model with tabular salt canopy, along ∼NE–SW. These stresses range between −150 and 300 units of stress. Almost half of the model area shows no build-up of shear stress (Fig. 4b). At and around the eastern and western edges of the tabular salt body, the shear stresses are higher (∼ −50 to −150 and ∼100 to 300 units of stress; Fig. 4b). In particular, at the periphery of the salt body immediately outside and inside it, there are lobes of significantly high shear stresses, ∼ −100 to −150 and 150 to 300 units of stress near both the western and eastern edges of the salt body (Fig. 4b). As noted earlier, we expect these areas to be more prone to earthquakes.

We now consider the entire extent of the salt bodies in our model and Figs 4(c) and (d) show the contours of shear stress after tectonic loading of 1 yr. Fig. 4(c) shows the contours of shear stress obtained after a ∼NW–SE tectonic loading. The shear stresses range between −150 and 150 units of stress (Fig. 4c). The shear stresses in most of the areas within the model, including some regions inside the salt body, vary within ∼0 and ±25 units of stress (Fig. 4c). However, there are pockets of relatively high shear stresses immediately outside the northern edge of the salt body (∼75 units of stress), at and along the southern edge of the salt body both inside and outside it (∼±75 to ±150 units of stress), and immediately to the west and east of the West Florida escarpment near its junction with the salt body (∼±50 units of stress) (Fig. 4c). In Fig. 4(d), we show the shear stress contours obtained after tectonic loading of the model along ∼NE–SW. These stresses range between −80 and 120 units of stress. Predominantly there is no or little stress build-up within most parts of the model (∼0 to −20 units of stress; Fig. 4d). However, there are some areas within the model where we obtain relatively high shear stresses. Among these areas is a lobe of significantly high shear stress (∼ −40 to −80 units of stress) at the northern edge of the salt body near its periphery (Fig. 4d). We also obtain pockets of relatively high shear stresses (∼±40–±60 units of stress) near the southwestern edge of the salt body, both inside and outside it (Fig. 4d). In addition, near the eastern edge of the salt body close to its junction with West Florida escarpment, shear stresses are heavily concentrated (∼ −40 to −60 and 60–120 units of stress; Fig. 4d). As mentioned before, these relatively high shear stress locations have the greatest potential to cause earthquakes.

We discuss the tectonic implications of our modelling results later. Next, we present our 3-D model of northern GOM and the results of its tectonic loading. We emphasize that these models are simplistic and are only aimed to test the hypothesis introduced earlier in this paper.

Three-dimensional model

Although one can test any hypothesis related to earthquakes using a 2-D model, a 3-D model, albeit simple, is more apt for the purpose. The obvious reason is that all earthquakes have a third dimension associated with them, their focal depths. Therefore, to test our hypothesis in three dimensions, we construct a simple 3-D model of northern GOM using the distinct element method implemented in '3DEC'. Our model (Fig. 5a) includes the tabular salt canopy (Fig. 2a), the outline of which in plan view is shown in Figs 2(b) and 5(b). The tabular salt canopy is surrounded by sediments. Due to intricacies of 3-D model construction using '3DEC', our model does not exactly replicate the tabular salt canopy outline in Fig. 2(b). However, the differences are minor and do not affect the results of modelling. To minimize boundary effects on the region of interest, we extend the block boundaries substantially away from it resulting in a total model area of ∼1300 km^2 (Fig. 5a). In our model, the tabular salt canopy and sediments surrounding it extend from the surface to a depth of ∼20 km. In the GOM, the depths of the salt bodies are highly variable. An important reason for this is our inadequate knowledge of the bottom of the salt, since salt presents a significant challenge to seismic imaging even with using advanced migration techniques. The focal depths of the earthquakes in the northern GOM are largely unconstrained but are thought to lie within 15 km. So that our 3-D model-calculated stresses (which we compare with locations of earthquakes in the depth dimension) due to the presence of the salt are not affected by boundary effects we arbitrarily choose the depth of the salt canopy to be 20 km, well past the predicted seismogenic depth. We assume elastic half-space below 20 km depth. Our model is deformable and we divide it into tetrahedral finite-difference zones using the built-in automatic mesh generator in '3DEC'.

To drive our model, we load them tectonically along the three mutually orthogonal stress directions (maximum horizontal stress, S_{Hmax}, minimum horizontal stress, S_{hmin}, and vertical stress, S_{v}) (Fig. 5a). In the case study of borehole breakout data from the Eugene Island Block 330, offshore Louisiana, in GOM, Peška & Zoback (1995) inferred that at a depth of ∼2 km, the upper bound of the magnitude of S_{Hmax} is ∼43 MPa, S_{hmin} is ∼37.1 MPa and S_{v} is ∼43 MPa. We assume these values to be representative of those in our study area and use them to load our model. Peška & Zoback (1995) also inferred that the orientation of S_{hmin} was between N36°E and N49°E. For simplicity, in our model we consider S_{hmin} to be oriented ∼N45°E and therefore S_{Hmax} is oriented ∼N45°W (Fig. 5a). S_{v}, in our model is oriented vertically (along the depth dimension) (Fig. 5a). Due to limitations in '3DEC' we rotate our model including the salt body 45° counter-clockwise such that S_{Hmax} is oriented ∼E–W (Fig. 5a). These loading stresses will in effect vary with depth. However, to our knowledge there is no site-specific stress profile that describes their variation with depth, and the focal depths of the earthquakes in GOM are also largely unconstrained. Moreover, we re-emphasize that our choice of linear, elastic and isotropic model causes the absolute values of computed stresses to scale almost linearly with respect to the values of the loading stresses, but their relative values at different locations within the model which are more important for the purpose of this study, remain unchanged. Therefore, we assume that the values of loading stresses are constant throughout the third dimension. We do however, include in our modelling, the effect of the increasing weight of overburden with depth.

The input parameters of our 3-D model are same as those of our 2-D models described earlier. Following Tuncay & Ortoleva (2001), we use bulk and shear moduli of 80 and 10 GPa, respectively, and density of 2000 kg m^{-3} for the tabular salt canopy in our model. For the surrounding sediments, we use a shear modulus of 13.23 GPa, density of 1781 kg m^{-3} (Huerta-Lopez *et al.* 2003), and along with these values use a Poisson's ratio of 0.32 (Huerta-Lopez *et al.* 2003) to derive the bulk modulus (33.65 GPa). We use values of normal and shear stiffnesses for the boundary of the tabular salt canopy based on laboratory studies of typical samples, assign a friction value of 0.5 to it, and assume it to be cohesionless. In our 3-D model, we use a linear, elastic and isotropic constitutive relation to define

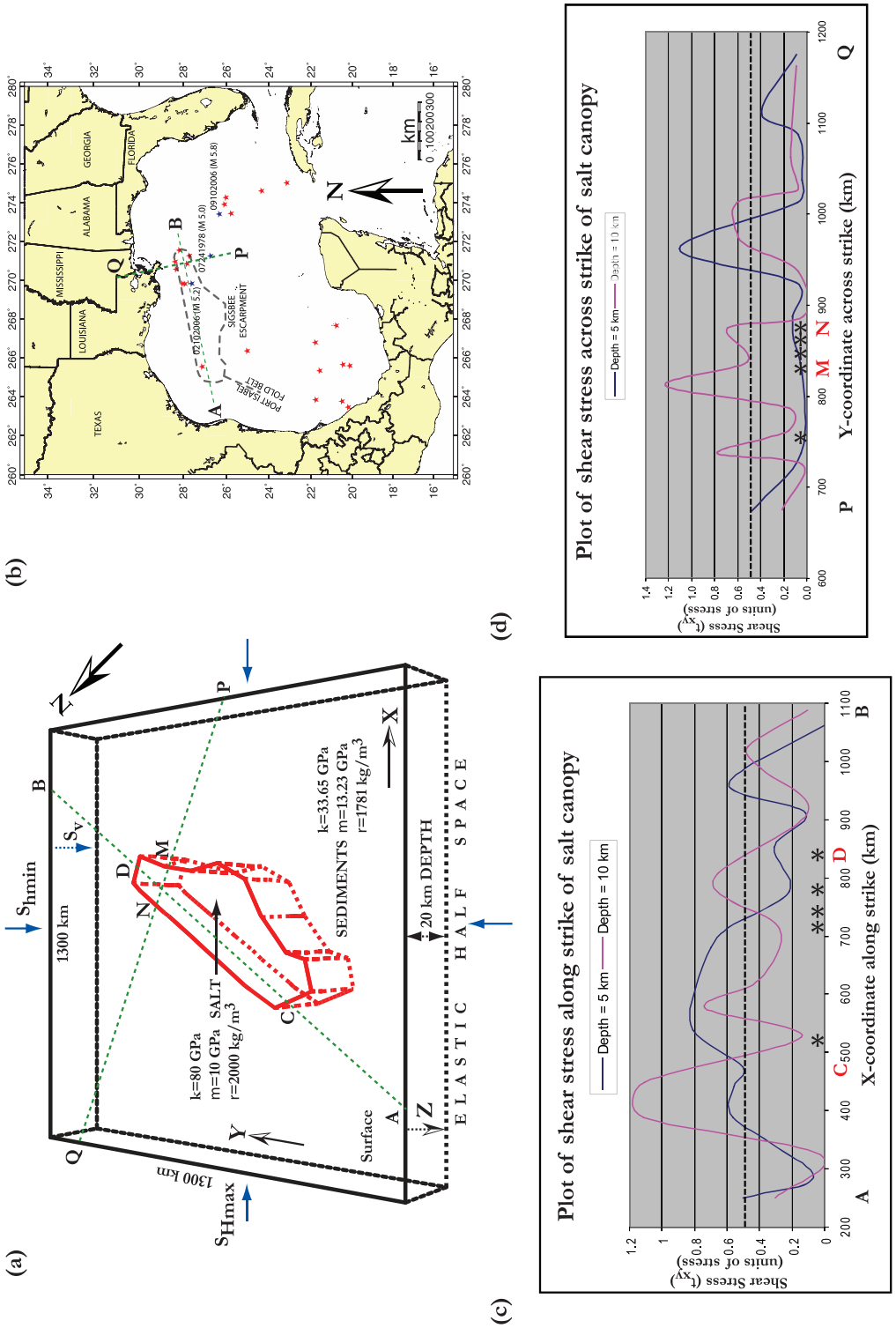

Figure 5. (a) Perspective view of the 3-D model geometry constructed using 3DEC of the tabular salt canopy (red outline; Gulf of Mexico Basin Depositional Synthesis Project (GBDS)'— Galloway 2006) surrounded by sediments. The solid lines indicate the outlines at the surface and the dotted lines indicate those at a depth of 20 km, below which the model assumes an elastic half-space. The material properties of salt and sediments used in the modelling are also indicated. The solid arrows (blue) indicate the three mutually orthogonal loading directions used in the modelling. The green broken lines indicate the profiles along, and across-strike of the salt canopy along which shear stresses (τ_{xy}) in (c) and (d) are plotted. (b) Map of Gulf of Mexico showing the outline of the tabular salt canopy, locations of earthquakes (following Fig. 2b), and profiles A–B and P–Q (green broken lines) for reference. Shear stresses in the x–y plane at 5 and 10 km depths obtained after a tectonic loading period of 1 yr are plotted along-strike (c), and across-strike (d) of the salt canopy. The broken lines in (c) and (d) indicates the arbitrarily chosen 0.5 units of stress for reference. The locations C, D, M and N correspond to locations along the profiles where they meet the edges of the salt canopy as shown in (a). The stars in (c) and (d) indicate projected locations of the earthquakes along the profiles.

the material behaviour of the tabular salt canopy and surrounding sediments. For the boundary of the salt body, we use a Coulomb Slip Failure relationship. We run our model for a tectonic loading time of 1 yr, and analyse the resulting shear stresses in particular observation planes at different depths, which we describe next.

Results of three-dimensional modelling

We report the resulting shear stresses (τ_{xy}) in the model after a tectonic loading of 1 yr. The focal depths of the earthquakes in northern GOM are largely unconstrained due to inadequate data. However, for the 2006 September 10 earthquake, the estimated focal depth was ∼10 km (United States Geological Survey—National Earthquake Information Center 2006). Therefore, from our 3-D modelling results we plot the absolute values of shear stresses at ∼5 and ∼10 km depths along profiles parallel to length (along-strike; profile A–B), and perpendicular to length (across-strike; profile P–Q) of the salt canopy (Fig. 5a). We also choose these profiles such that their locations encompass those of the earthquakes in northern GOM (Fig. 5b). For convenience of comparison, we project the locations of the earthquakes along the profiles. We re-emphasize that the magnitudes of shear stress obtained in this study are insignificant but their relative values at different locations within the models are instructive. We present the results below and discuss their tectonic implications later.

Fig. 5(c) shows the distribution of shear stresses along profile A–B which runs parallel to the length (along-strike) of the salt canopy (Fig. 5a). The shear stresses range between ∼0 and ∼1.2 units of stress. Along the profile A–B at a depth of 5 km, the shear stresses are higher (∼0.5–0.9 units of stress) between ∼375 and 730 km and ∼930 and 980 km, respectively (Fig. 5c; blue curve). At most of the other locations along profile A—B, the shear stresses at 5 km depth are within ∼0.1–0.5 units of stress (Fig. 5c; blue curve). At a depth of 10 km, however, there are pockets of elevated shear stresses along the profile A–B (Fig. 5c; magenta curve). Within these pockets, the shear stresses are ∼0.5–1.2 units of stress between ∼350 and 500 km, ∼0.5–0.75 units of stress between ∼560 and 620 km, ∼0.5–0.7 units of stress between ∼750 and 830 km and ∼0.5 units of stress at ∼1000 km along the profile A–B (Fig. 5c; magenta curve). At a depth of 5 km, the shear stress at the end A of the profile is relatively high (∼0.5 units of stress) due to the effect of the model edge, and is ignored as an artefact.

In Fig. 5(d), we show the distribution of shear stresses along profile P–Q which runs perpendicular to the length (across-strike) of the salt canopy (Fig. 5a). The shear stresses range between ∼0.1 and ∼1.25 units of stress. Along the profile P–Q at a depth of 5 km, the shear stresses are higher (∼0.5–1.1 units of stress) between ∼930 and 1000 km (Fig. 5d; blue curve). At most of the other locations along profile P–Q, the shear stresses at 5 km depth are between ∼0—and 0.4 units of stress, except for the end P where it is 0.5 units of stress (Fig. 5d; blue curve). The elevated stress at end P is due to edge effect and is ignored as an artefact. As observed earlier along the along-strike profile, at a depth of 10 km there are local pockets of stress concentration also along profile P–Q which runs across-strike of the salt canopy (Fig. 5d; magenta curve). Within these pockets the shear stresses are ∼0.5–0.8 units of stress between ∼725 and 760 km, ∼0.5–1.25 units of stress between ∼800 and 880 km and ∼0.5–0.7 units of stress between ∼960 and 1020 km along the profile P–Q (Fig. 5d; magenta curve). The shear stresses elsewhere along profile P–Q at 10 km depth are below 0.5 units of stress.

Next, we discuss the tectonic implications of our 2-D and 3-D modelling results.

DISCUSSIONS

Analytical studies by Campbell (1978) showed that contrast in mechanical properties between intrusions and surrounding host rocks concentrates stress around the periphery of the intrusions and inside them when subjected to background tectonic loading (Fig. 1d). He also suggested that this stress concentration could lead to earthquakes. Ben-Zion (2001), Ben-Zion & Huang (2002), Brietzke & Ben-Zion (2006) and Ampuero & Ben-Zion (2008) also concluded similarly from their numerical simulations and case studies. As described earlier, using the 'distinct element method' implemented through commercially available computer programmes, we demonstrate this phenomenon (Figs 1a–c). Next, we test the applicability of this phenomenon to explain the seismicity of the northern GOM, using simple 2-D and 3-D models generated by the same method and computer programmes. Analogous to the examples studied by Campbell (1978), in our models we consider the salt deposits to be intrusions and surrounding sediments to be the host rocks, and the background stress field provides the external loading force. Figs 4(a)–(d) and 5(c) and (d) show the results of our modelling. The magnitudes of the shear stresses obtained from the model results have no actual significance since they depend on the model parameters, but their relative values are instructive and we use them for tectonic interpretations. We make a tacit assumption that the seismicity pattern is representative of the distribution of stresses. Comparing the shear stress distribution within the models (Figs 4a–d), and along the chosen profiles (Figs 5c and d), with the locations of the earthquakes in northern GOM, we observe good spatial correspondence in their general patterns, irrespective of the orientations of S_{Hmax}.

(1) From our 2-D and 3-D modelling results, a general observation that shear stresses are relatively elevated near the periphery of the salt bodies and also within it in some locations (Figs 4a–d and 5c and d), supports the results of analytical studies of Campbell (1978) (Figs 1a–d), and numerical simulations of Ben-Zion (2001), Ben-Zion & Huang (2002), Brietzke & Ben-Zion (2006) and Ampuero & Ben-Zion (2008). Therefore, the phenomenon that in the presence of background tectonic loading, stress concentration occurs due to contrast in mechanical properties between intrusions and surrounding host rocks leading to earthquakes (which is the hypothesis that we set out to test in this study), holds promise as a possible cause of the seismicity in northern GOM.

(2) With the 2-D models comprising the tabular salt canopy, for either orientations of S_{Hmax} we observe in our modelling results some spatial association of locations of relatively high shear stresses with those of the seismicity in northern GOM (Figs 4a and b). This spatial association is particularly strong for the earthquakes near the western edge of the tabular salt canopy (Figs 4a and b). However, the earthquakes near the eastern edge of the tabular salt canopy have a strong spatial association with locations of elevated stresses in the case of ∼NE–SW orientation of S_{Hmax}, but not as strong when the S_{Hmax} is oriented ∼NW–SE (Figs 4a and b). This observation implies that these earthquakes (some of which are historical) for which reliable focal mechanisms do not exist due to lack of data availability may have been caused by a ∼NE–SW oriented stress field. We note earlier that the orientation of stress field in northern GOM is highly variable due to local perturbations. The 2006

February 10 (red star) and 1978 July 24 (blue star) earthquakes both are spatially associated with areas of relatively high stresses (within the error bounds of their epicentral locations) irrespective of the orientation of S_{Hmax} although their values are higher when S_{Hmax} is oriented ∼NE–SW than when it is oriented ∼NW–SE (Figs 4a and b). The focal mechanism of the 1978 July 24 earthquake though implies that the causative S_{Hmax} was oriented ∼NW–SE, that of the 2006 February 10 event (Fig. 2b) has poor constraints and is not definitive (Pulliam 2006, personal communication).

(3) When the 2-D models consist of the entire extent of the salt bodies, we observe in our modelling results good spatial association of some of the locations of elevated stresses with that of most of the earthquakes, including the ones in 1978 and 2006, for either orientations of S_{Hmax} (Figs 4c and d). The cluster of earthquakes that are close to and aligned with the location of the West Florida escarpment (including the 2006 September 10 earthquake) is associated with nearly equally stressed areas for either orientations of S_{Hmax} (Figs 4c and d). The earthquakes near the southern edge of the salt body (including the 2006 February 10 event) are associated with slightly higher stresses when S_{Hmax} is oriented ∼NW–SE than when it is oriented ∼NE–SW (Figs 4c and d). Our modelling results also indicate that with this geometry of the salt body and orientation and nature of S_{Hmax}, areas along the southern edge of the salt body exhibit extensive strike-slip motion compared to other locations. We also obtain some strike-slip motion along the West Florida escarpment. Therefore, these areas are more likely to fail causing earthquakes than other areas. The distribution of earthquakes in northern GOM (Figs 4c and d) attests to this fact. This observation is also consistent with the compressive nature of S_{Hmax} which causes either strike-slip or reverse movements. The focal mechanism of the 2006 February 10 event (Fig. 2c; Pulliam 2006, personal communication) has a strong strike-slip component and is consistent with this observation. The most reliable focal mechanism of the 1978 July 24 earthquake implies primarily thrust faulting but there are other end-member focal mechanisms for the earthquake that fit the data equally well and have strong strike-slip components (Frohlich 1982), consistent with our observations. Due to the 2-D nature of these results, we are unable to duplicate reverse movements.

(4) The results of our 3-D modelling studies further support the spatial association of locations of relatively high shear stresses with earthquakes in the northern GOM. At either depths, the values of shear stresses increase considerably in the vicinity and at and/or near the periphery of the tabular salt canopy and within it (Figs 5c and d), consistent with the analytical studies of Campbell (1978), Ben-Zion (2001), Ben-Zion & Huang (2002), Brietzke & Ben-Zion (2006) and Ampuero & Ben-Zion (2008), thereby suggesting that the phenomenon we test in this study may very well be in play in the northern GOM. Also at a depth of 5 km, immediately past the western edge of the tabular salt canopy along profile A–B (point C in Fig. 5c), shear stresses increase and remain elevated well inside the salt body (Fig. 5c; blue curve). In contrast at a depth of 10 km, except for a small pocket of elevated shear stresses, they are generally very low (Fig. 5c; magenta curve). The shear stresses within the salt body close to its eastern edge at a depth of 5 km (Fig. 5c; blue curve) are lower, whereas those at a depth of 10 km are relatively elevated (Fig. 5c; magenta curve). This observation implies that it is most likely that the focal depth of the earthquake near the western end of the salt body (whose location coincides with that of elevated stresses at a depth of 5 km) is shallow. On the contrary, some of the earthquakes near the eastern end of the salt body whose locations coincide with those of higher stresses at only 10 km depth, have possibly occurred around that depth. The 2006 February 10 event is located within an envelope of elevated stresses at a depth of 5 km (Fig. 5c; blue curve), thereby suggesting its shallow source around that depth. At the time when this manuscript was in review, an independent study in conjunction with the United States Geological Survey (USGS; Dewey & Dellinger 2008) also had a similar conclusion.

(5) The distribution of shear stresses along profile P–Q is also insightful regarding possible focal depths of the earthquakes in northern GOM. At a depth of 5 km, shear stresses are only elevated north of the northern edge of the tabular salt canopy (Fig. 5d; blue curve) implying that seismicity in that area is likely to be shallow. Within the tabular salt canopy between its northern and southern edges, shear stresses along profile P–Q are relatively large at a depth of 10 km but not at 5 km (Fig. 5d). This observation corroborates a similar one from shear stresses along profile A–B whereby the earthquakes in this area are potentially deeper. In addition, we also note that the shear stresses along profile P–Q are larger at a depth of 10 km at the location of the 1978 July 24 earthquake (Fig. 5d; magenta curve) suggesting a deeper source for the event, consistent with the ∼15 km depth obtained by Frohlich (1982).

(6) Our study shows that shear stresses build-up within the salt body and some of their locations correlate well with those of earthquakes in the northern GOM. However, it is widely known that salt is mechanically weak and flows (Hudec & Jackson 2007). Therefore, the question arises whether or not shear failure can occur within a salt body. In a study to assess salt mechanics, Fossum & Fredrich (2002) discussed various factors influencing shear failure in salt when it is allochthonous in nature. The tabular salt canopy in the epicentral area of the northern GOM is allochthonous as opposed to autochthonous (Orange *et al.* 2004), implying thereby that under appropriate conditions brittle failure can occur within the salt body. On the issue of being mechanically weak, we note that irrespective of whether the salt bodies are stronger or weaker than the sediments surrounding them, concentration of stresses occur within them and around their peripheries. This observation has been discussed earlier with case studies of intrusions by Campbell (1978), Gangopadhyay (2005) and Stevenson *et al.* (2006). Therefore, the choice of contrast in mechanical properties either way does not affect the main conclusion of this study.

CONCLUSIONS

In this study, we set out to test the hypothesis that contrast in mechanical properties between the salt bodies and surrounding sediments may be a possible cause of the seismicity in northern GOM. Our study comes in the wake of three earthquakes in 2006 that occurred in the region which is relatively aseismic. We successfully demonstrate using 2-D and 3-D mechanical modelling that the phenomenon may indeed be a player in causing occasional earthquakes in northern GOM. Our study also provides important insights into the nature of the local stress field that may promote seismic activity in the area. Given the inadequate constraints on the focal depth of important earthquakes in the region, we are able to comment on the preferred locations of these sources. We intend to draw attention to this study from the hydrocarbon exploration community to invest resources to further conduct detailed site-specific investigations related to this phenomenon.

ACKNOWLEDGMENTS

We thank the editor, Dr Yehuda Ben-Zion, and two anonymous reviewers for their constructive comments that helped improve this manuscript. We also thank Drs Joseph Dellinger and Meredith Nettles, organizers of the workshop on the 2006 GOM earthquakes during the Annual Meeting of the SEG, for inviting us to present our study. Abhijit Gangopadhyay thanks Dr Pradeep Talwani, and the University of South Carolina for allowing access to the commercial numerical modelling codes used in this study. He also thanks Dr Mrinal K. Sen for providing financial support to attend the SEG workshop. We thank Drs Cliff Frohlich, Yosio Nakamura, Jay Pulliam and Pradeep Talwani for their insightful comments during preparation of this manuscript. Financial support for this work was provided in part by the John A. and Katherine G. Jackson School of Geosciences and the Geology Foundation. A figure in this manuscript was made using the Generic Mapping Tools (GMT) software (Wessel & Smith 1991).

Abhijit Gangopadhyay dedicates this manuscript to the loving memory of his father who left for his heavenly abode on 2007 May 24, while this work was ongoing.

REFERENCES

3DEC, 2003. *Three Dimensional Distinct Element Code, Version 3.0*. ITASCA Corporation, Minnesota, Minneapolis, USA.

Ampuero, J.-P. & Ben-Zion, Y., 2008. Cracks, pulses and macroscopic asymmetry of dynamic rupture on a bimaterial interface with velocity-weakening friction, *Geophys. J. Int.,* **173,** 674–692.

Barton, N., 1976. The shear strength of rock and rock joints, *Int. J. Rock Mech. Min. Sci. Geomech. (Abstract),* **13,** 255–279.

Ben-Zion, Y., 2001. Dynamic rupture in recent models of earthquake faults, *J. Mech. Phys. Solids,* **49,** 2209–2244.

Ben-Zion, Y. & Huang, Y., 2002. Dynamic rupture on an interface between a compliant fault zone layer and a stiffer surrounding solid, *J. geophys. Res.,* **107,** doi:10.1029/2001JB000254.

Bird, D.E., Burke, K., Hall, S.A. & Casey, J.F., 2005. Gulf of Mexico tectonic history: hotspot tracks, crustal boundaries, and early salt distribution, *Am Assoc. Petrol. Geol. Bull.,* **89,** 311–328.

Brietzke, G.B. & Ben-Zion, Y., 2006. Examining tendencies of in-plane rupture to migrate to material interfaces, *Geophys. J. Int.,* **167,** 807–819.

Campbell, D.L., 1978. Investigation of the stress-concentration mechanism for intraplate earthquakes, *Geophys. Res. Lett.,* **5,** 477–479.

Cundall, P.A., 1971. A computer model for simulating progressive, large scale movement in blocky rock systems, in *Proceedings of Symposium on Rock Fracture, International Society of Rock Mechanics*, Nancy I, Paper II-8.

Dewey, J.W. & Dellinger, J.A., 2008. Location of the Green Canyon (Offshore Southern Louisiana) Seismic Event of February 10, 2006, *Open-File Report 2008-1184*, United States Geological Survey, pp. 30.

Dokka, R.K., 2006. Modern-day tectonic subsidence in coastal Louisiana, *Geology,* **34,** 281–284.

Dokka, R.K., Sella, G.F. & Dixon, T.H., 2006. Tectonic control of subsidence and southward displacement of southeast Louisiana with respect to stable North America, *Geophys. Res. Lett.,* **33,** L23308, doi:10.1029/2006GL027250.

Donnell, L.H., 1941. Stress concentrations due to elliptical discontinuities in plates under edge forces, in *Theodore von Karman Anniversary Volume,* pp. 293–309, California Institute of Technology, Pasadena.

Fossum, A.F. & J.T. Fredrich, 2002. Salt mechanics primer for near-salt and sub-salt deepwater Gulf of Mexico field developments, *Report prepared by Sandia National Laboratories*, pp. 67.

Frohlich, C., 1982. Seismicity of the central Gulf of Mexico, *Geology,* **10,** 103–106.

Galloway, W., 2006. Map—Gulf of Mexico Structure, Gulf Basin Depositional Synthesis Project (GBDS), The University of Texas at Austin.

Gangopadhyay, A., 2005. Mechanisms of continental intraplate earthquakes, *Ph.D dissertation*. University of South Carolina, pp. 253.

Gangopadhyay, A., 2006. Re-visiting the tectonics of the oceanic intraplate earthquake of March 25, 1998 (M 8.1) in the Balleny Sea, offshore Antarctica, *Earth Planet. Sci. Lett.,* **249,** 456–466.

Gangopadhyay, A., Dickerson, J. & Talwani, P., 2004. A two-dimensional numerical model for the current seismicity in New Madrid Seismic Zone, *Seism. Res. Lett.,* **75,** 406–418.

Hall, S.A. & Najmuddin, I.J., 1994. Constraints on the tectonic development of the eastern Gulf of Mexico provided by magnetic anomaly data, *J. geophys. Res.,* **99,** 7161–7175.

Hudec, M.R. & Jackson, M.P.A., 2007. Terra infirma: understanding salt tectonics, *Earth Sci. Rev.,* **82,** 1–24.

Huerta-Lopez, C., Pulliam, J. & Nakamura, Y., 2003. *In situ* evaluation of shear-wave velocities in seafloor sediments with a broadband ocean-bottom seismograph, *Bull. Seism. Soc. Am.,* **93,** 139–151.

Marton, G. & Buffler, R.T., 1994. Jurassic reconstruction of the Gulf of Mexico Basin, *Int. Geol. Rev.,* **36,** 545–586.

Matava, T., 2006. A petroleum systems study of the northern Gulf of Mexico, *Leading Edge,* **25,** 478–482.

Nettles, M., 2006. Two unusual seismic events in the Gulf of Mexico in 2006, in *Proceedings of Incorporated Research Institutions in Seismology (IRIS) Annual Workshop (Abstracts)*.

Nettles, M., 2007. Analysis of the 10 February 2006: Gulf of Mexico Earthquake from Global and Regional Seismic Data, in *Proceedings of Annual Conference*, Offshore Technology Conference, Houston, Texas.

Nunn, J.A., 1985. State of stress in the northern Gulf Coast, *Geology,* **13,** 429–432.

Orange, D.L., Angell, M.M., Brand, J.R., Thomson, J., Buddin, T., Williams, M., Hart, W. & Berger III, W.J., 2004. Geologic and shallow salt tectonic setting of the Mad Dog and Atlantis fields: relationship between salt, faults, and seafloor geomorphology, *Leading Edge,* **23,** 354–365.

Pan, J. *et al*., 2006. Depth imaging and regional exploration in Northeast Garden Banks, Gulf of Mexico, *Leading Edge,* **25,** 468–473.

Peška, P. & Zoback, M.D., 1995. Compressive and tensile failure of inclined well bores and determination of in situ stress and rock strength, *J. geophys. Res.,* **100,** 12 791–12 811.

Pindell, J.L., 1985. Alleghenian reconstruction and subsequent evolution of the Gulf of Mexico, Bahamas and proto-Caribbean, *Tectonics,* **4,** 1–39.

Reed, J.M., 1994. Probable cretaceous-to-recent rifting in the gulf of Mexico Basin, an answer to Callovian salt deformation and distribution problems? Part 1, *J. Petrol. Geol.,* **17,** 429–444.

Reed, J.M., 1995. Probable cretaceous-to-recent rifting in the Gulf of Mexico Basin, an answer to Callovian salt deformation and distribution problems? Part 2, *J. Petrol. Geol.,* **18,** 49–74.

Reinecker, J., Heidbach, O., Tingay, M., Sperner, B. & Müller, B., 2005. The release 2005 of the World Stress Map (available online at www.world-stress-map.org).

Rosso, R.S., 1976. A comparison of joint stiffness measurements in direct shear, triaxial compression, and *in situ, Int. J. Rock Mech. Min. Sci. Geomech. (Abstract),* **13,** 167–172.

Salvador, A., 1991. Origin and development of the Gulf of Mexico Basin, in *The Gulf of Mexico Basin,* pp. 389–344, ed. Salvador, A., Geological Society of America (*The Geol. North Am.*, J).

Sarwar, G., 2002. Northern Gulf of Mexico: a passive or passive active margin? in *Proceedings of the AAPG Annual Meeting (Abstracts)*. American Association of Petroleum Geologists.

Stevenson, D., Gangopadhyay, A. & Talwani, P., 2006. Booming Plutons: source of microearthquakes in South Carolina, *Geophys. Res. Lett.,* **33,** L03316, doi:10.1029/2005GL024679.

Talwani, P. & K. Rajendran, 1991. Some seismological and geometric features of intraplate earthquakes, *Tectonophysics,* **186,** 19–41.

Tingay, M., Müller, B., Reinecker, J., Heidbach, O., Wenzel, F. & Fleckenstein, P., 2005. Understanding tectonic stress in the oil patch: the World Stress Map Project, *Leading Edge,* **24,** 1276–1282.

Tuncay, K. & Ortoleva, P., 2001. Salt tectonics as a self-organizing process: a reaction, transport, and mechanics model, *J. geophys. Res.,* **106,** 803–817.
UDEC, 1999. *Universal Distinct Element Code, Version 3.1,* ITASCA Corporation, Minneapolis, Minnesota, USA.
United States Geological Survey, National Earthquake Information Center, 2006. Preliminary Determination of Epicenters (PDE).
Wessel, P. & Smith, W.H.F., 1991. Free software helps map and display data, *EOS, Trans. Am. geophys. Un.,* **72,** 441.
White, G.W., 1980. Permian-Triassic continental reconstruction of the Gulf of Mexico-Caribbean area, *Nature,* **283,** 823–826.
Winker, C.D. & Buffler, R.T., 1988. Paleogeographic evolution of early deep-water Gulf of Mexico and margins, Jurassic to middle Cretaceous (Comanchean), *Am. Assoc. Petrol. Geol. Bull.,* **72,** 318–346.

APPENDIX

The distinct element method in UDEC and 3DEC uses an explicit finite-difference scheme to solve the equations of motion for the blocks in the model (3DEC 2003). It performs the computations in the time-domain at every time step. For a particular model, it decides the time step automatically using a stability criterion that requires the velocities and accelerations to be constant during the chosen time step. The time step therefore, is a function of the stiffnesses of the blocks and faults (discontinuities) in the model (3DEC 2003). At each time step, it applies Newton's law of motion and the prescribed constitutive relations to all the nodes (gridpoints or vertices of the zones). At each node, the equations of motion are

$$\ddot{u}_i = \left[\int_s \sigma_{ij} n_j \mathrm{d}s + F_i\right]/m + g_i, \tag{1}$$

where, s is the surface enclosing the mass, m, assumed to be located at the node, n_j is the unit normal to s, F_i is the resultant of all external forces at the node, g_i is the gravitational acceleration and σ_{ij} is the stress at a point on the surface, s.

The resultant of all external forces at each node, F_i, is

$$F_i = F_i^{\mathrm{z}} + F_i^{\mathrm{c}} + F_i^{\mathrm{l}}, \tag{2}$$

where, F_i^{l} represents the external applied loads, F_i^{c} represents the contact forces that exist only for nodes along the block boundary, and the contribution of the internal stresses in the zones adjacent to the node is F_i^{z} which is given by

$$F_i^{\mathrm{z}} = \int_c \sigma_{ij} n_j \mathrm{d}s, \tag{3}$$

where, σ_{ij} is the zone stress tensor, and n_j is the outward unit normal to the contour c. Finally, it calculates a net nodal force vector, ΣF_i, which includes the above contributions and also those from the body forces due to gravity. If the model is in equilibrium, ΣF_i at the node will be zero, otherwise, the node will be accelerated according to the finite-difference form of Newton's second law of motion given by

$$(\mathrm{d}u_i/\mathrm{d}t)^{(t+\Delta t/2)} = (\mathrm{d}u_i/\mathrm{d}t)^{(t-\Delta t/2)} + \Sigma F_i^{(t)}(\Delta t/m), \tag{4}$$

where the superscripts denote the time at which the corresponding variable is evaluated. During each time step, the programme computes the strains and rotations (which are related to the nodal displacements) as

$$\varepsilon_{ij} = {}^1\!/_2(u_{i,j} + u_{j,i}), \tag{5}$$

$$\theta_{ij} = {}^1\!/_2(u_{i,j} - u_{j,i}). \tag{6}$$

It also uses the constitutive relation for deformable blocks at each time step in the following form,

$$\Delta\sigma_{ij}^{\mathrm{e}} = \lambda\Delta\varepsilon_v\delta_{ij} + 2\mu\Delta\varepsilon_{ij}, \tag{7}$$

where, λ and μ are the Lame's constants, $\Delta\sigma_{ij}^{\mathrm{e}}$ are the elastic increments of the stress tensor, $\Delta\varepsilon_{ij}$ are the incremental strains, $\Delta\varepsilon_v$ is the increment of volumetric strain and δ_{ij} is the Kronecker delta function. The cycle repeats itself for the specified duration of the model run.

The distinct element method in UDEC and 3DEC allows the user to apply either a stress (load) or displacement (velocity) boundary condition to the model (3DEC 2003). It applies the condition to the centroid of the blocks along the boundary for a rigid block model. For deformable blocks, it specifies displacements in terms of prescribed velocities at the nodes and does not invoke eq. (4) at those nodes. At a stress boundary, it derives the forces according to the following equation,

$$F_i = (\sigma_{ij}^{\mathrm{b}} n_j)\Delta s, \tag{8}$$

where, n_j is the outward normal vector of the boundary segment, and Δs is the length of the boundary segment over which the stress, σ_{ij}^b, acts. It then adds the force, F_i, into the force summation in eq. (1) for the appropriate nodes (3DEC 2003). A factor of concern in using the distinct element method is the representation of the far-field boundary, particularly in the case of representing an unbounded medium by a finite-numerical model. The formulation of the distinct element method in UDEC and 3DEC requires that the faults (discontinuities) not remain isolated and have to extend to the block boundaries. This could give rise to anomalous stress concentrations near the block boundaries which could interfere with the stress concentrations in the area of interest in the model. A simple way of avoiding this situation is by building the model in such a way that the region of interest is adequately away from the block boundaries. Additionally, this problem is also addressed when using a linear, elastic and isotropic model, wherein the block assembly is coupled to a boundary-element representation of the far field (3DEC 2003).